Histol Histopathol (2025) 40: 757-772

Histology and Histopathology
From Cell Biology to Tissue Engineering

ORIGINAL ARTICLE Open Access

Ameliorative effects of HGF-overexpressed exosomes derived from ADMSCs on oxidative stress in hepatic fibrosis

Hanyu Zhou, Yanyan Wu, Junchao Xue and Liushenyan Yu

Department of Pharmacy, Tongde Hospital of Zhejiang Province, Xihu District, Hangzhou City, Zhejiang Province, PR China

Summary. Background. Hepatic fibrosis, ultimately causing hepatic sclerosis, remains significant health concerns. Adipose-derived mesenchymal stem cell (ADMSC)-derived exosomes (Exo) exhibit amelioration of liver injury. Hepatocyte growth factor (HGF) regulates hepatocyte growthn. However, its involvement during hepatic fibrosis remains unclear.

Methods. Isolation of ADMSCs and Exo, transfection of HGF overexpression, and activation of hepatic stellate cells (HSCs) by Angiotensin II (AngII) were conducted. Cells were randomized into HSC, AngII-HSC, ADMSCs-Exo, ADMSCs^{blank}-Exo, and ADMSCs^{HGF}-Exo, DPI, LY294002, and SB203580 groups. MTT for cell viability, cell migration, and flow cytometry for ROS were performed. BALB/c mice were treated with CCL4 for hepatic fibrosis models. The mice were randomized into Control, PBS, ADMSCs-Exo, ADMSCs^{blank}-Exo, and ADMSCs^{HGF}-Exo groups (n=6). HE, Sirius red, and Oil Red O staining, liver function indicators, and ELISA for oxidative stress were performed. ROS generation-related and PI3K/Akt/P38MAPK-related factors were detected by immunofluorescence, immunohistochemistry, and western blot.

Results. After identification of ADMSC-Exo and transfection, AngII increased cell viability, migration, Collagen I (CoLI), α-smooth muscle actin (α-SMA), ROS, NADPH oxidase 4 (NOX4), PI3K, p-Akt, p-P38MAPK, ras-related C3 botulinum toxin substrate 1 (RAC1), p47^{phox}, and p22^{phox} expression. However, ADMSCs^{HGF}-Exo, DPI, LY294002, and SB203580 reversed the above effects. Moreover, ADMSCs^{HGF}-Exo inhibited pathological damage, fibrosis, lipid accumulation, ALT, AST, TBIL, CoLI, α-SMA, NOX4, MDA, PI3K, P-Akt, and P-P38MAPK expression, and increased ALB, SOD, GPx, CAT, GSH, Mn-SOD, Na^+-K^+-ATPase, and Ca^{2+}-Mg^{2+}-ATPase levels in hepatic fibrosis mice.

Conclusion. ADMSCs^{HGF}-Exo attenuated hepatic fibrosis by inhibiting oxidative stress through activating the PI3K/Akt/P38MAPK pathway, providing valuable insights for potential treatment of liver fibrosis.

Key words: Hepatic fibrosis, ADMSCs, Exo, HGF, Oxidative stress

Introduction

Liver fibrosis results from the excessive deposition of diffuse extracellular matrix (ECM) during the repair of chronic liver injury (Cordero-Espinoza and Huch, 2018). The activation of hepatic stellate cells (HSCs) plays a pivotal role in the development and progression of liver fibrosis. Typically, liver fibrosis is a response to persistent liver damage caused by various factors such as viral hepatitis, alcohol abuse, or cholestatic liver disease (Qiu et al., 2019; Shiha et al., 2020). Elevated oxidative stress levels characterize the early stages of liver fibrosis development and progression (Atallah et al., 2018). Studies have shown that liver fibrosis is a major contributor to cirrhosis and hepatocellular carcinoma, with approximately 90% of hepatocellular carcinomas developing based on liver fibrosis or cirrhosis (Chen et al., 2020; Liu et al., 2020). Left untreated, liver fibrosis

Corresponding Author: Liushenyan Yu, Department of Pharmacy, Tongde Hospital of Zhejiang Province, No. 234, Gucui Road, Xihu District, Hangzhou City, 310012, Zhejiang Province, PR China. e-mail: yu274032964@126.com

www.hh.um.es. DOI: 10.14670/HH-18-816

Abbreviation. ADMSCs: Adipose-derived mesenchymal stem cells; α-ALB: albumin; SMA: α-Smooth muscle actin; ALT: alanine aminotransferas; AngII: Angiotensin II; AST: aspartate transaminase; CAT: catalase; CoLI: Collagen I; ECM: extracellular matrix; Exo: Exosomes; GFP: green fluorescent protein; GPx: glutathione peroxidase; GSH: glutathione; HGF: hepatocyte growth factor; hHGF: human HGF; HSCs: hepatic stellate cells; MDA: malondialdehyde; mHGF: mouse HGF; Mn-SOD: manganese superoxide dismutase; NTA: nanoparticle tracking analysis; NOX4: NADPH oxidase 4; RAC1: ras-related C3 botulinum toxin substrate 1; SOD: superoxide dismutase; SPF: specific pathogen-free; TBIL: total bilirubin; TGFBR2: transforming growth factor beta receptor 2

can progress to decompensated cirrhosis, leading to severe complications and posing a significant threat to individuals and society (Asrani et al., 2019).

Adipose-derived mesenchymal stem cells (ADMSCs) are increasingly recognized as promising seed cells for cell therapy and tissue engineering (Dubey et al., 2018). ADMSCs possess enhanced self-renewal ability, immunomodulatory function, and convenient extraction characteristics, making them valuable in alleviating the liver inflammatory response and injury, being widely employed in liver injury repair, and have been shown to significantly improve liver function in research studies (Saidi et al., 2015; Deng et al., 2016). Liu et al. (2023) revealed that ADMCs downregulated alanine aminotransferase (ALT), aspartate aminotransferase (AST), total bilirubin (TBIL), and α-Smooth muscle actin (α-SMA) levels of CCL4-induced liver fibrosis in rats, thereby mitigating liver collagen deposition and liver fibrosis. ADSCs highly express CD44 and CD105 but not CD34 and CD45 (Wang et al., 2019). Moreover, ADSCs exert important anti-oxidative stress and anti-apoptotic properties for ameliorating liver injury (Sorgun and Erbaş, 2023). It was found that ADSCs decreased malondialdehyde (MDA) and transforming growth factor-β (TGF-β) levels and inhibited oxidative stress and inflammatory responses in liver-injured rats (Sorgun and Erbaş, 2023).

The therapeutic mechanism of ADMSCs is closely linked to the paracrine formation of exosomes (Exo) (Watanabe et al., 2019). Exo contain regulatory substances identical to those found in parent cells, such as lipids, proteins, DNA, and miRNA, which can interact with and act on target cells through paracrine secretion from MSCs (Yao et al., 2019). It has been revealed that hepatocyte growth factor (HGF) secreted by ADMSCs is one of the factors responsible for the therapeutic effects of Exo (Ross et al., 2012). HGF, acting as a ubiquitous and broadly acting factor, inhibits hepatocyte apoptosis and promotes liver regeneration (Yin et al., 2013). A recent study further indicated that HGF overexpression in MSCs significantly enhanced their anti-fibrotic capacity (Hu et al., 2020a).

In this study, we investigated the modulatory effect of ADMSCs^{HGF}-Exo on oxidative stress in liver fibrosis through *in vivo* and *in vitro* experiments.

Materials and methods

Cell culture

The rat hepatic stellate cell HSC-T6 cells (iCell-r014, iCell) were inoculated in DMEM medium containing 10% fetal bovine serum at conditions of 37°C and 5% CO_2.

Animals

Thirty healthy 6- to 8-week-old specific pathogen-free (SPF)-grade male BALB/c mice, weighing approximately 18-25 g, and five healthy three-week-old SPF female BALB/c mice were acquired from Shanghai SLAC Laboratory Animal Co., Ltd under license No. SCXK (Hu) 2017-0005. Of these, five female mice were used for subsequent isolation and identification of ADMSCs, while the remaining 30 mice were employed to establish the models. The Zhejiang Eyong Pharmaceutical R&D Co., Ltd maintained these mice in an environment with a constant temperature of 22±2°C, 50-60% constant humidity, a light/dark cycle of 12h, and air changes of 15-20 times per hour. All mice had free access to water and food. All experimental procedures were conducted following protocols approved by the Institutional Animal Care and Use Committee at the Animal Experimentation Ethics Committee of Zhejiang Eyong Pharmaceutical Research and Development Center (SYXK-(Zhe)-2021-0033).

Isolation of ADMSCs

The extraction and isolation of ADMSCs were performed as per the previous study (Zedan and Al-Ameri, 2023). Subcutaneous adipose tissue debridement and extraction were performed on five three-week-old SPF female BALB/c mice from the medial inguinal region. Following washing the adipose tissue with PBS, 5 mL of type I collagenase was added, with continuous agitation at 37°C for 1h. Subsequently, centrifugation was performed at 2000 rpm for 5 min. The cells obtained were resuspended in DMEM/F12 with 100 mg/L fetal bovine serum and 10 g/L Penicillin/Streptomycin. The cells were centrifuged at 1000 rpm for 5 min and the supernatant discarded. ADMSCs were inoculated at a density of 2×10^5/mL in DMEM/F12 medium containing 10% fetal bovine serum and incubated in a CO_2 incubator. After 24h, the medium change was performed, followed by medium changes every three days thereafter. When the cells reached 90% confluence, they were passaged, digested with 0.25% trypsin for about 1 min, and the morphology of cells from different generations was observed under a microscope. Identification of ADMSCs was made by flow cytometry.

Extraction of Exo

Exo extraction was carried out following the steps of the previous study (Xiong et al., 2023). The serum medium containing ADMSCs was centrifuged at 100,000 r/min for 70 min at 4°C. After 24h of incubation in conditioned medium (DMEM/F12+10% Exo-removed serum), the cell culture supernatant was collected and centrifuged at 800 r/min at 4°C for 10 min. Then this was centrifuged at 100,000 r/min for 70 min at 4°C to remove cell debris and apoptotic vesicles. Subsequently, the gain of Exo precipitate was performed by centrifugation at 10,000 r/min for 20 min at 4°C, filtration through a 0.22 μm membrane, and 100,000 r/min for 70 min at 4°C. After the addition of PBS and centrifugation at 100,000 r/min for 70 min, the

supernatant was discarded to obtain purified ADMSC-Exo, which were resuspended by adding 100 mL of sterile PBS and kept at -20°C.

Cell transfection

Two lentiviral vectors, a blank lentiviral vector encoding only green fluorescent protein (GFP), and a human HGF (hHGF)-expressing lentiviral vector encoding GFP were obtained from Shanghai Genechem Company (GOSL49905). Log-phase ADMSCs were selected for cell transfection. At 24h before lentiviral transfection, the adherent cells were inoculated into 24-well plates at 1×10^5 per well so that the number of cells at the time of lentiviral transfection was approximately 2×10^5/well. The next day, DMEM/F12 was replaced with 2 mL of fresh medium containing 6 μg/mL polybrene. When the cell density reached 70%, infection with overexpressed lentivirus was performed by adding the virus suspension at an infection multiplicity of 50 and a viral titer of 10^8 IU/mL, and incubation was continued for 24h at 37°C. The medium containing the virus was then replaced with fresh medium, continuing incubation for 72h. Subsequently, Exo from ADMSCs, $ADMSCs^{blank}$, and $ADMSCs^{HGF}$ groups were isolated using the ultra-centrifugation technique. The morphology of isolated Exo was examined by electron microscopy (Motic, AE2000), and Exo particle size and concentration were determined by nanoparticle tracking analysis (NTA).

qRT-PCR assay

ADMSCs were lysed using TRIzol (B511311, Sangon Biotech (Shanghai) Co. Ltd), and total RNA from ADMSCs, $ADMSCs^{blank}$, and $ADMSCs^{HGF}$ was extracted. Subsequently, reverse transcription was performed using the CW2569 reverse transcription kit (Kangwei Shiji), followed by PCR amplification using the SYBR Green qPCR kit (CW2601, Kangwei Shiji). The level of *HGF* mRNA was calculated using the $2^{-\Delta\Delta Ct}$ method, with β-actin serving as the internal reference. The gene primer sequences are provided in Table 1.

Cell activation and grouping

HSC-T6 cells were resuspended in DMEM containing 10% serum, and their cell morphology was inspected. After 2 or 3 days, the medium was replaced with complete medium containing ADMSCs-Exo, $ADMSCs^{blank}$-Exo, and $ADMSCs^{HGF}$-Exo, respectively, while the control group received complete medium. Two days later, HSC-T6 cells were directly treated with DMEM containing Angiotensin II (AngII, 1 μmol/L, HY-13948, MCE) for activation (Yanan et al., 2023). The cells were assayed after two days of culture. The experimental groups included HSC Control, AngII-HSC, AngII-HSC + ADMSCs-Exo, AngII-HSC + $ADMSCs^{blank}$-Exo, and AngII-HSC + $ADMSCs^{HGF}$-Exo groups. Additionally, HSCs were pre-stimulated with the NOX inhibitor DPI (D2926, Sigma, 20 μmol/L) (Mohamed et al., 2019), the PI3K/Akt signal pathway inhibitor LY294002 (440202, Sigma, 10 μmol/L) (Hu et al., 2020b), and the P38MAPK signal pathway inhibitor SB203580 (S8307, Sigma, 10 μmol/L) (Mo et al., 2020) for 30 min. They were then treated with an AngII (1 μmol/L) working solution. Therefore, the cell treatments were grouped as AngII-HSC + DPI, AngII-HSC + LY294002, and AngII-HSC + SB203580.

MTT assay

Cells from each group were inoculated in 96-well plates at a density of 1×10^4 cells/mL, 200 μL per well, and cultured for 24h. Subsequently, 20 μL of MTT solution (1 mg/mL, BBI Life Sciences, E606334) was added to each well and incubated for 4h. After discarding the culture solution, 200 μL/well of DMSO was added and shaken for 10 min. The absorbance value at 595 nm was detected. Cell activity=(absorbance value of experimental group - absorbance value of blank group)/(absorbance value of control group - absorbance value of blank group)×100%. Each experiment was repeated three times.

Cell scratch assay

Lines were drawn approximately every 0.5 cm to 1 cm intervals by a marker pen on the back of the six-well plates. Each well was crossed at least three lines. Approximately 5×10^5 cells were added to each well and incubated overnight, scratched with a gun tip perpendicularly to the lines, washed three times with PBS, and incubated for 24h. Photographs were obtained and recorded at 0h and 24h. Cell migration rate=(0h scratch width - 24h scratch width) / 0h scratch width × 100%.

Cell migration assay

After adjusting the cell concentration to 5×10^5/mL, 100 μL of cell suspension was added to the upper

Table 1. qPCR Primer sequences.

Gene	Forward Primer	Reverse Primer
Mouse *HGF*	GGTTACAGGGGAACCAGCAA	TCGGATGTTTGGGTCAGTGG
Human *HGF*	GCACTGACTCCGAACAGGAT	CAGGAGGAGATGCAGGAGGA
β-actin	GGGAAATCGTGCGTGAC	AGGCTGGAAAAGAGCCT

chamber of a Transwell, and 500 μL of medium was added to the lower chamber, and incubated at 37°C 5% CO_2 for 24h. The bottom cells of the upper chamber were wiped off with cotton swabs, and Transwell chambers were fixed with 4% paraformaldehyde for 10 min. After washing three times with PBS, it was immersed in 0.1% crystal violet staining solution for 30 min and washed with PBS. After drying, the cells were observed under the microscope, and five fields of view were randomly selected for photographing and calculating the number of cells migrating into the lower chamber by ImageJ software.

Immunofluorescence assay

HSC-T6 cells from each group were inoculated in 24-well plates at a density of 2×10^5 cells/mL, 1 mL per well, and cultured for 24h. Each well was fixed with 1 mL of 4% paraformaldehyde for 10 min, washed three times with PBS, and then blocked by the addition of 3% BSA for 30 min. Subsequently, primary antibodies, including anti-α-SMA (Abcam, ab5831), anti-Collagen I (CoLI, Abcam, ab260043), anti-ROS (Santa Cruz, sc-376217), and anti-NADPH oxidase 4 (NOX4, Abcam, ab109225) antibodies were added to incubate at 4°C overnight. The next day, the cells were washed with PBS and labeled with fluorescent secondary antibodies for 2h at 37°C. After washing with PBS, the nuclei were stained with DAPI and observed by fluorescence microscopy. Images were visualized with a Nikon inverted fluorescence microscope (Ts2-FC, Shanghai, China) using the CFI60 Infinity Optical System and were captured by a ToupView CMOS digital camera with a pixel size of 4.63×4.63 μm.

Flow cytometry

After adjusting the cell concentration to 5×10^6/mL, 100 μL of cells were mixed well with the corresponding antibodies: CD105 (562759, BD), CD34 (551387, BD), CD44 (553134, BD), and CD45 (560695, BD) and incubated at room temperature away from light for 15 min. Following washing with PBS and centrifugation to remove the supernatant, 500 μL of PBS was added for flow cytometer assessment (C6, BD).

ROS detection: Cells from each group were inoculated in six-well plates at a density of 1×10^4 cells/mL, and the cell culture medium was removed after the corresponding treatment. Diluted DCFH-DA (10 μmol/L, 1 mL) was then added and incubated for 20 min at 37°C. Cells were washed three times with serum-free culture medium to adequately remove the DCFH-DA that did not enter the cells and flow cytometry measurement was performed.

Establishment of an acute liver injury mouse model and therapeutic grouping

The mouse liver injury model was established using the CCL4 composite modeling method (He et al., 2023). Twenty-four mice were selected as liver fibrosis models, while six served as normal controls. On the first day of modeling, each mouse received subcutaneous injections of 40% CCL4-olive oil solution at 5 mL/kg. Subsequently, on the second and following days, the animals were weighed and received subcutaneous injections of 40% CCL4-olive oil at 3 mL/kg twice a week for six weeks. This was accompanied by a high-fat, low-protein diet (fat:protein:carbohydrates = 60%:20%:20%) and 0.5% alcohol as drinking water. The control group received an equal volume of olive oil at each injection and was fed a normal diet (fat:protein:carbohydrates = 11%:23%:66%) with water.

The mice were randomly divided into five groups: normal controls (Control), PBS, ADMSCs-Exo, $ADMSCs^{blank}$-Exo, and $ADMSCs^{HGF}$-Exo (n=6). As of the third week of modeling, $ADMSCs^{HGF}$-Exo, $ADMSCs^{blank}$-Exo, and ADMSCs-Exo were injected via the tail vein (400 μg/μL, 200 μL) as the experimental group once a week until the end of the sixth week of modeling (Luo et al., 2023). Liver-injured mice injected with the same amount of PBS served as the untreated PBS group, and normal mice were used as the control group. The gross morphology of the liver was observed and serum biochemical indexes were measured to assess the effects of modeling. After 24h of mouse modeling, blood was extracted from the abdominal aorta, allowed to stand at room temperature for 3h, and then centrifuged at 3000 r/min for 10 min, thereby collecting the upper serum. Euthanasia was performed by carbon dioxide inhalation and liver tissues were collected. One part of the collected liver tissue was fixed with 4% paraformaldehyde and sectioned by paraffin embedding, and the other part was kept at -80°C.

ELISA

The levels of Na^+-K^+-ATPase, Ca^{2+}-Mg^{2+}-ATPase, ALT, AST, albumin (ALB), and TBIL in mouse serum were measured using Na^+-K^+-ATPase, Ca^{2+}-Mg^{2+}-ATPase, ALT (Shanghai Enzyme-linked Biotechnology Co., Ltd., ML063179), AST (Shanghai Enzyme-linked Biotechnology Co., Ltd., ML058577), ALB (Shanghai Enzyme-linked Biotechnology Co., Ltd., ML057991), and TBIL (Nanjing Jiancheng, C019-1-1) ELISA kits.

Fully automated biochemistry test

The levels of MDA, superoxide dismutase (SOD), glutathione peroxidase (GPx), catalase (CAT), glutathione (GSH), and manganese superoxide dismutase (Mn-SOD) in mouse serum were measured using a fully automated biochemical instrument (Abbott Laboratories, C16000).

HE staining

Mouse liver tissue samples were placed in a 4%

paraformaldehyde solution and paraffin sections were prepared. The sections were soaked in xylene solution for dewaxing and subsequently placed in gradient ethanol solution (anhydrous ethanol for 2 min, 95% for 1 min, 80% for 1 min, 75% for 1 min, and distilled water for 2 min). Subsequently, hematoxylin (MDL, MD911467) staining was performed for 5 min, tap water rinsing for 5 min, hydrochloric acid ethanol differentiation for 30 s, and tap water immersion for 15 min, followed by eosin (Zhuhai Beso Biotechnology Co., Ltd., 613101) staining for 2 min. After gradient ethanol dehydration, xylene for transparency was added and slices were sealed. Observations were made with a fluorescence microscope (Leica, DM3000).

Sirius red staining

Prepared paraffin sections of mouse liver tissues were soaked in xylene solution for dewaxing and subsequently placed in gradient ethanol solution (anhydrous ethanol for 2 min, 95% for 1 min, 80% for 1 min, 75% for 1 min, and distilled water for 2 min). Subsequently, the sections were stained in Sirius red staining solution (Wuhan Google, G1018) for 8 min, rinsed in anhydrous alcohol, oven-dried at 60°C, clearing in xylene for 5 min, sealed, and observed under a microscope (Leica, DM3000). ImageJ software was utilized for analysis and calculation of the ratio of positive-stained area to total area.

Oil Red O staining

Following fixation for 24h, mouse liver tissues were sequentially dehydrated by placing them into 15% and 30% sucrose solution at 4°C. Subsequently, OCT embedding agent was added dropwise around the tissues, snap-frozen, embedded, sectioned (8-10 μm), and stored at -20°C for later use. The frozen sections were rewarmed and dried, fixed for 15 min, washed with water, and air-dried. Then sections were immersed in Oil Red O dye solution for 8-10 min, protected from light, removed, and immersed into two vats of 60% isopropanol and two vats of pure water for differentiation and immersion washing, each for 3 s, 5 s, 10 s, and 10 s. Hematoxylin re-staining for 3-5 min, with three vats of pure water immersion washes, 5 s, 10 s, and 30 s each. The samples were differentiated with differentiation solution for 2-8 s, washed in two tanks of distilled water for 10 s each, returned to blue solution for 1 s, and gently immersed in two tanks of tap water for 5 s and 10 s. After observing staining by microscopic examination, the slices were sealed. The ratio of positive staining area to total area was calculated by ImageJ software.

Immunohistochemistry assay

Prepared sections of mouse liver tissues were taken and baked at 60°C for 1h, and then xylene and gradient alcohol were added. Sections were placed in citrate buffer repair solution (0.1 mol/L, pH=6.0), microwaved for 10 min, cooled naturally, and washed with PBS. Subsequently, 3% H_2O_2 was added and incubated for 10 min, then left at room temperature for 30 min. Overnight incubation with primary antibodies, including anti-CoLI (Abcam, ab260043), anti-α-SMA (Abcam, ab5831), and anti-NOX4 (Abcam, ab109225) at 4°C was carried out, with incubation of secondary antibody at room temperature for 20 min the next day. DAB chromogen (MDL, MD912068) was used to develop color, with hematoxylin re-staining, dehydration, transparency, and neutral gum sealer. The sections were sealed and examined under a microscope (Leica, DM3000).

Western blot

The levels of CD9, CD63, and CD81 in Exo, the levels of ras-related C3 botulinum toxin substrate 1 (RAC1), $p47^{phox}$, $p22^{phox}$, P-I3K, P-Akt, and P-P38MAPK in the HSCs, and the levels of CoLI, α-SMA, NOX4, P-I3K, P-Akt, and P-P38MAPK in the mouse liver tissues were measured by western blot. Total protein in Exo, HSCs, and mouse liver tissues was collected, and the total protein concentration was detected using the BCA protein kit (Solarbio, PC0020). We blocked the PVDF membrane with 5% skim milk powder, incubated the membrane with primary antibodies CD9 (Abcam, ab92726), CD63 (Abcam, ab68418), CD81 (Santa Cruz, sc-9158), RAC1 (Abcam, ab155938), $p47^{phox}$ (Abcam, ab166930), $p22^{phox}$ (Santa Cruz, sc-271968), CoLI (Abcam, ab34710), α-SMA, NOX4 (Affinity, DF6924), P-I3K (Affinity, AF6242), P-Akt (Abcam, ab8805), and P-P38MAPK (Affinity, AF4001) overnight. The membrane was then rinsed and incubated with HRP. Protein bands were detected by ECL, and the gray protein value was calculated using ImageJ software. GAPDH served as the internal reference.

Statistical analysis

Statistical analysis was performed using SPSS statistical software. One-way ANOVA was applied for multiple groups, followed by Tukey's test for comparison between groups. The Kruskal–Wallis H test was employed for variance heterogeneity. All data are expressed as mean ± standard deviation (SD), where $p<0.05$ indicates that the difference is statistically significant.

Results

Transfection of ADMSCs with HGF resulted in high HGF expression

In Fig. 1a, the morphology of ADMSCs was characterized by rapid growth and a significant

proportion of cells having a fibrous or spindle shape. The percentage of cells positive for ADMSC surface molecular markers CD44 and CD105 was found to be more than 90%, with molecular markers CD34 and CD45 both being negative, below 1% (Fig. 1b). After successful transfection, mouse HGF (mHGF) and hHGF levels in the ADMSCs and ADMSCs^{blank} group were not significantly different, while the ADMSCs^{HGF} group exhibited significantly higher expression levels of both mHGF and hHGF (Fig. 1c, $p<0.01$).

Transfection of ADMSC-Exo exhibited no effects on the stemness of ADMSCs

ADMSCs-Exo were isolated from ADMSCs, in which the hollow spherical macrovesicles were ADMSCs-Exo, and an NTA assay detected the particle size and Exo concentration (Fig. 2a). The expression of Exo surface markers CD9, CD63, and CD81 did not differ significantly among groups (Fig. 2b). The proportions of CD44- and CD105-positive cells in ADMSCs^{HGF} and ADMSCs^{blank} group cells were > 90%, and CD34- and CD45-positive cells were < 1% (Fig. 2c). Therefore, transfection did not affect the stemness of ADMSCs.

ADMSCs^{HGF}-Exo caused lower viability and migration in HSC-T6 cells

As derived from Fig. 3a, compared with the HSC group, the OD value and cell viability of HSC-T6 exhibited an increase in the AngII-HSC, AngII-HSC + ADMSCs-Exo, AngII-HSC + ADMSCs^{blank}-Exo, and AngII-HSC + ADMSCs^{HGF}-Exo groups ($p<0.01$). The HSC-T6 cell OD value and cell viability in the AngII-HSC + ADMSCs-Exo, AngII-HSC + ADMSCs^{blank}-Exo, AngII-HSC + ADMSCs^{HGF}-Exo, AngII-HSC + DPI, AngII-HSC + LY294002, and AngII-HSC + SB203580 groups was significantly lower than that in the AngII-HSC group ($p<0.05$ or $p<0.01$). As displayed in Fig. 3b,c, the migration ability of HSCs in the AngII-HSC, AngII-HSC + ADMSCs-Exo, AngII-HSC + ADMSCs^{blank}-Exo, AngII-HSC + ADMSCs^{HGF}-Exo, and AngII-HSC + DPI groups was significantly higher

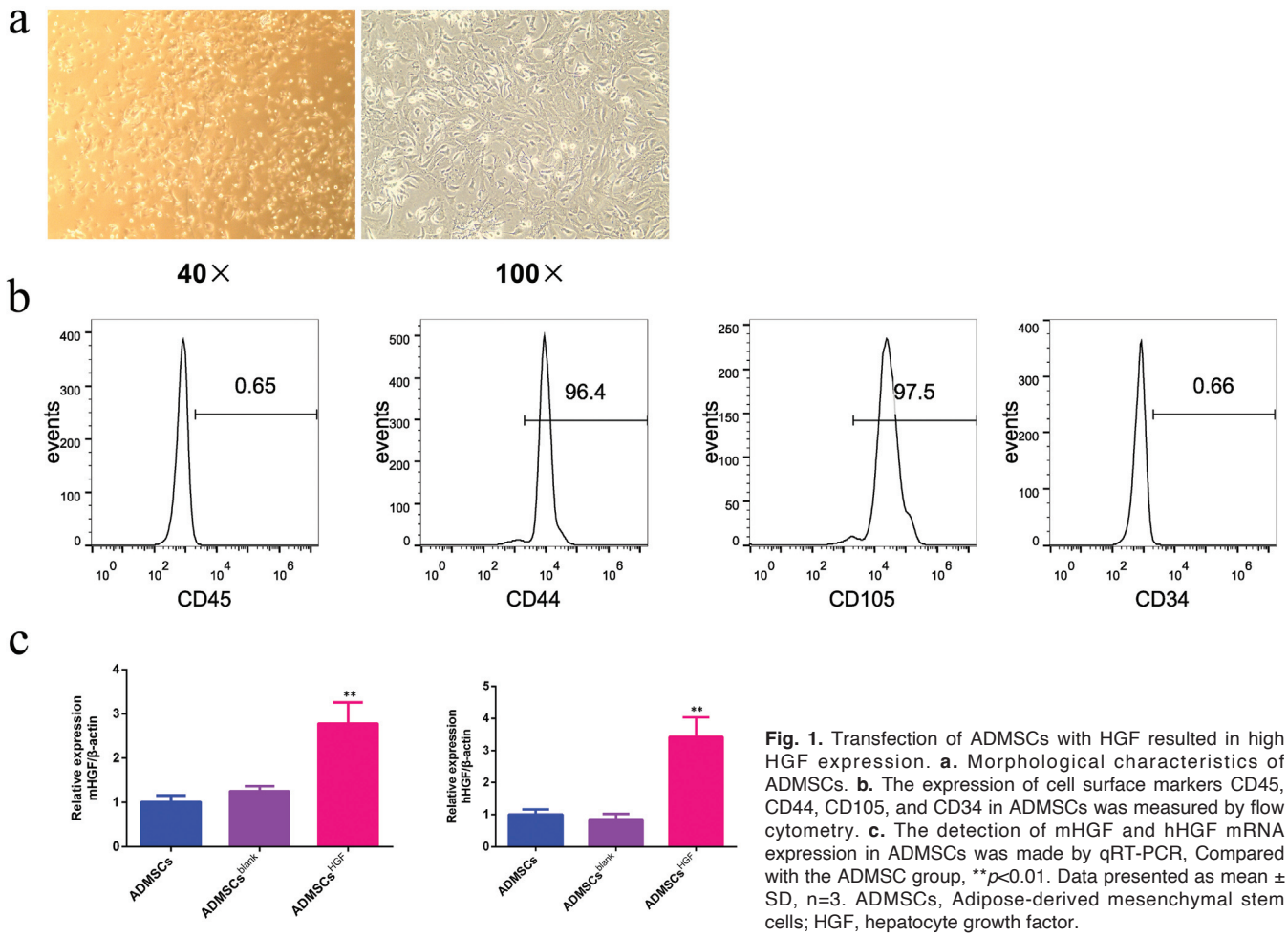

Fig. 1. Transfection of ADMSCs with HGF resulted in high HGF expression. **a.** Morphological characteristics of ADMSCs. **b.** The expression of cell surface markers CD45, CD44, CD105, and CD34 in ADMSCs was measured by flow cytometry. **c.** The detection of mHGF and hHGF mRNA expression in ADMSCs was made by qRT-PCR, Compared with the ADMSC group, $^{**}p<0.01$. Data presented as mean ± SD, n=3. ADMSCs, Adipose-derived mesenchymal stem cells; HGF, hepatocyte growth factor.

than in the HSC group ($p<0.05$ or $p<0.01$). Furthermore, the migration ability in the AngII-HSC + ADMSCs-Exo, AngII-HSC + ADMSCs^{blank}-Exo, AngII-HSC + ADMSCs^{HGF}-Exo, AngII-HSC + DPI, AngII-HSC + LY294002, and AngII-HSC + SB20358 groups was significantly reduced when compared with the AngII-HSC group ($p<0.05$ or $p<0.01$).

ADMSCs^{HGF}-Exo decreased CoLI, α-SMA, ROS, and NOX4 expression in HSC-T6 cells

According to Fig. 4, CoLI, α-SMA, ROS, and NOX4 expression was significantly higher in AngII-HSC, AngII-HSC + ADMSCs-Exo, AngII-HSC + ADMSCs^{blank}-Exo, and AngII-HSC + ADMSCs^{HGF}-

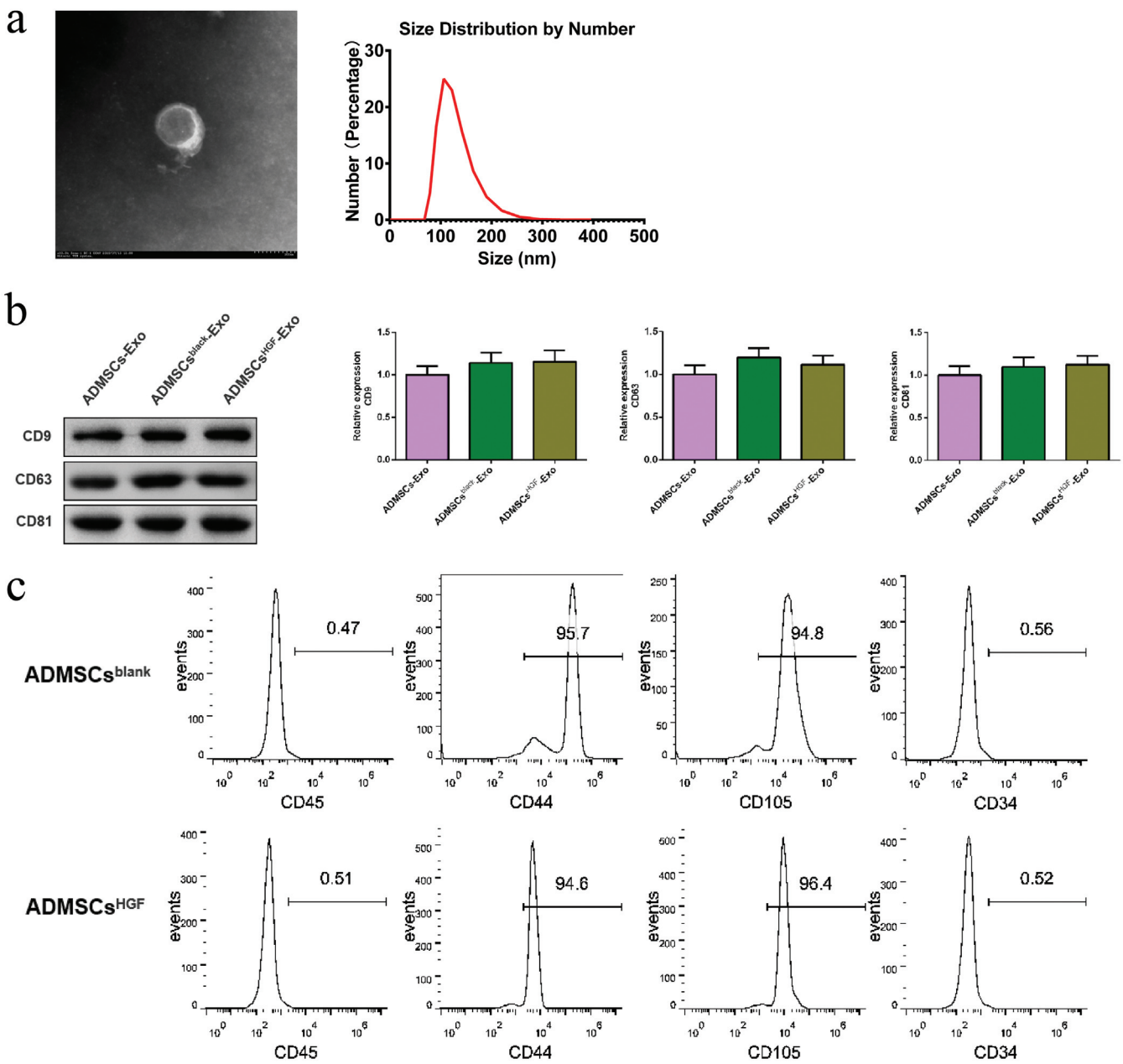

Fig. 2. Transfection of ADMSCs-Exo exhibited no effects on the stemness of ADMSCs. **a.** Exo morphology, particle size, and concentration were tested by electron microscopy and NTA assay. **b.** Expression of Exo surface markers (CD9, CD63, and CD81) was examined by western blot. **c.** Measurement of CD105, CD34, CD44, and CD45 cell surface marker expression in ADMSCs after HGF transfection was performed by flow cytometry. Data presented as mean ± SD, n=3. ADMSCs, Adipose-derived mesenchymal stem cells; HGF, hepatocyte growth factor; NTA: nanoparticle tracking analysis; Exo, exosomes.

Exo, AngII-HSC + DPI, AngII-HSC + LY294002, and AngII-HSC+SB20358 groups than that of HSC group ($p<0.05$ or $p<0.01$). Compared with the AngII-HSC group, CoLI, α-SMA, ROS, and NOX4 expression was lower in AngII-HSC + ADMSCs-Exo, AngII-HSC + ADMSCs^{blank}-Exo, and AngII-HSC + ADMSCs^{HGF}-Exo, AngII-HSC + DPI, AngII-HSC + LY294002, and AngII-HSC + SB20358 groups ($p<0.05$ or $p<0.01$). Moreover, compared with the AngII-HSC + ADMSCs^{blank}-Exo groups, AngII-HSC + ADMSCs^{HGF}-Exo exhibited lower α-SMA, ROS, and NOX4 expression ($p<0.05$ or $p<0.01$).

In Fig. 5, the fluorescence intensity of ROS in the AngII-HSC, AngII-HSC + ADMSCs-Exo, AngII-HSC + ADMSCs^{blank}-Exo, AngII-HSC + ADMSCs^{HGF}-Exo, AngII-HSC + DPI, AngII-HSC + LY294002, and AngII-HSC + SB203580 groups appeared significantly enhanced compared with the HSC group ($p<0.01$). In comparison with the AngII-HSC group, inhibition of ROS levels occurred in the AngII-HSC + ADMSCs-Exo, AngII-HSC + ADMSCs^{blank}-Exo, AngII-HSC + ADMSCs^{HGF}-Exo, AngII-HSC + DPI, AngII-HSC + LY294002, and AngII-HSC + SB20358 groups ($p<0.05$ or $p<0.01$). Interestingly, there was no significant difference in ROS levels among the AngII-HSC + ADMSCs-Exo, AngII-HSC + ADMSCs^{blank}-Exo, and AngII-HSC + ADMSCs^{HGF}-Exo groups.

ADMSCs^{HGF}-Exo inhibited ROS production by downregulation of P-I3K, P-Akt, and P-P38MAPK protein expression in HSC-T6 cells

The expression of ROS generation-related molecular proteins, including RAC1, p47^{phox}, and p22^{phox}, was higher in HSC-T6 cells of the AngII-HSC, AngII-HSC + ADMSCs-Exo, and AngII-HSC + ADMSCs^{blank}-Exo groups than that of the HSC group (Fig. 6a, $p<0.05$ or $p<0.01$). However, ROS production-related molecular

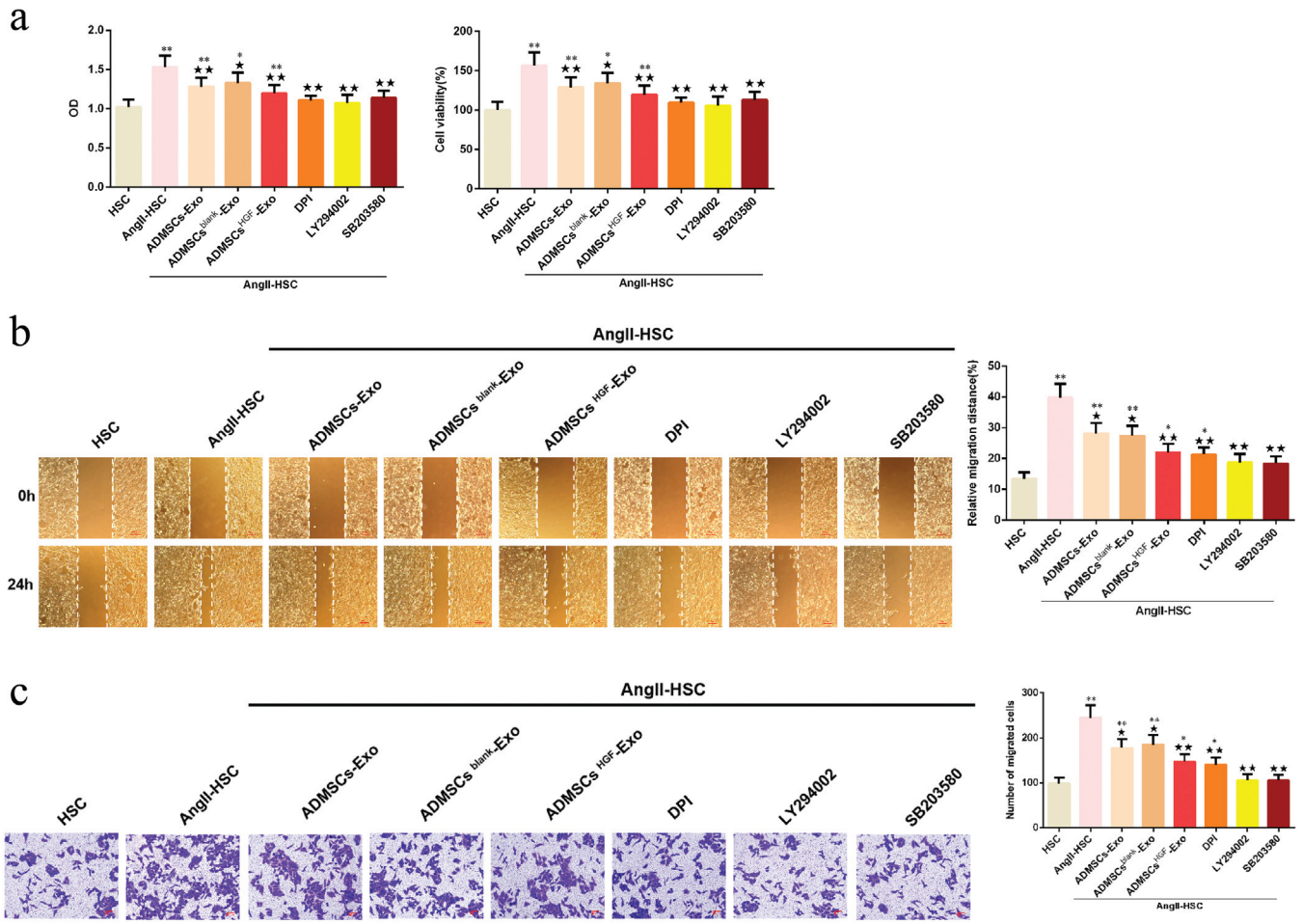

Fig. 3. ADMSCs^{HGF}-Exo caused lower viability and migration in HSC-T6 cells. **a.** The impact of ADMSCs^{HGF}-Exo on HSC viability was detected by the MTT method. Cell migration of HSCs was tested by cell scratch **(b)** and cell migration assays **(c)**. Data presented as mean ± SD, n = 6. Compared with the HSC group, *$p<0.05$, **$p<0.01$; Compared with the AngII-HSC group, ★$p<0.05$, ★★$p<0.01$. ADMSCs, Adipose-derived mesenchymal stem cells; HGF, hepatocyte growth factor; Exo, exosomes.

protein expression demonstrated a decrease in AngII-HSC + ADMSCs-Exo, AngII-HSC + ADMSCs^{blank}-Exo, AngII-HSC + ADMSCs^{HGF}-Exo, AngII-HSC + DPI, AngII-HSC + LY294002, and AngII-HSC + SB20358 groups when compared with the AngII-HSC group (p<0.05 or p<0.01). There was lower RAC1 protein expression in the AngII-HSC + ADMSCs^{HGF}-Exo group than in the AngII-HSC + ADMSCs^{blank}-Exo group (p<0.05). Interestingly, p47^{phox} and p22^{phox} expression in the AngII-HSC + ADMSCs-Exo, AngII-HSC + ADMSCs^{blank}-Exo, and AngII-HSC + ADMSCs^{HGF}-Exo groups exhibited no significant difference.

As demonstrated in Fig. 6b, the expressions of P-I3K, P-Akt, and P-P38MAPK were higher in all other groups than in the HSC group. Compared with the AngII-HSC group, the expression of P-I3K, P-Akt, and P-P38MAPK was decreased in HSCs of all groups except the HSC group (p<0.05 or p<0.01). The AngII-HSC + ADMSCs^{HGF}-Exo group exhibited reduced P-Akt and P-P38MAPK expression than in the AngII-HSC + ADMSCs^{blank}-Exo group (p<0.05 or p<0.01).

ADMSCs^{HGF}-Exo ameliorated liver function biochemical indicators, liver tissue injury, fibrosis, and lipid accumulation in CCL4-treated mice

The flowchart of the animal experiment is presented in Fig. 7a. As indicated in Fig. 7b, compared with control mice, the serum levels of ALT, AST, and TBIL were increased, with lowered ALB levels in the CCL4-treated mice of the PBS, ADMSCs-Exo, ADMSCs^{blank}-Exo, and ADMSCs^{HGF}-Exo groups (p<0.05 or p<0.01). Serum levels of ALT, AST, and TBIL in the ADMSCs-Exo, ADMSCs^{blank}-Exo, and ADMSCs^{HGF}-Exo groups were lower, whereas ALB levels increased compared with the PBS group (p<0.05 or p<0.01). Relative to the ADMSCs^{blank}-Exo group, ADMSCs^{HGF}-Exo had

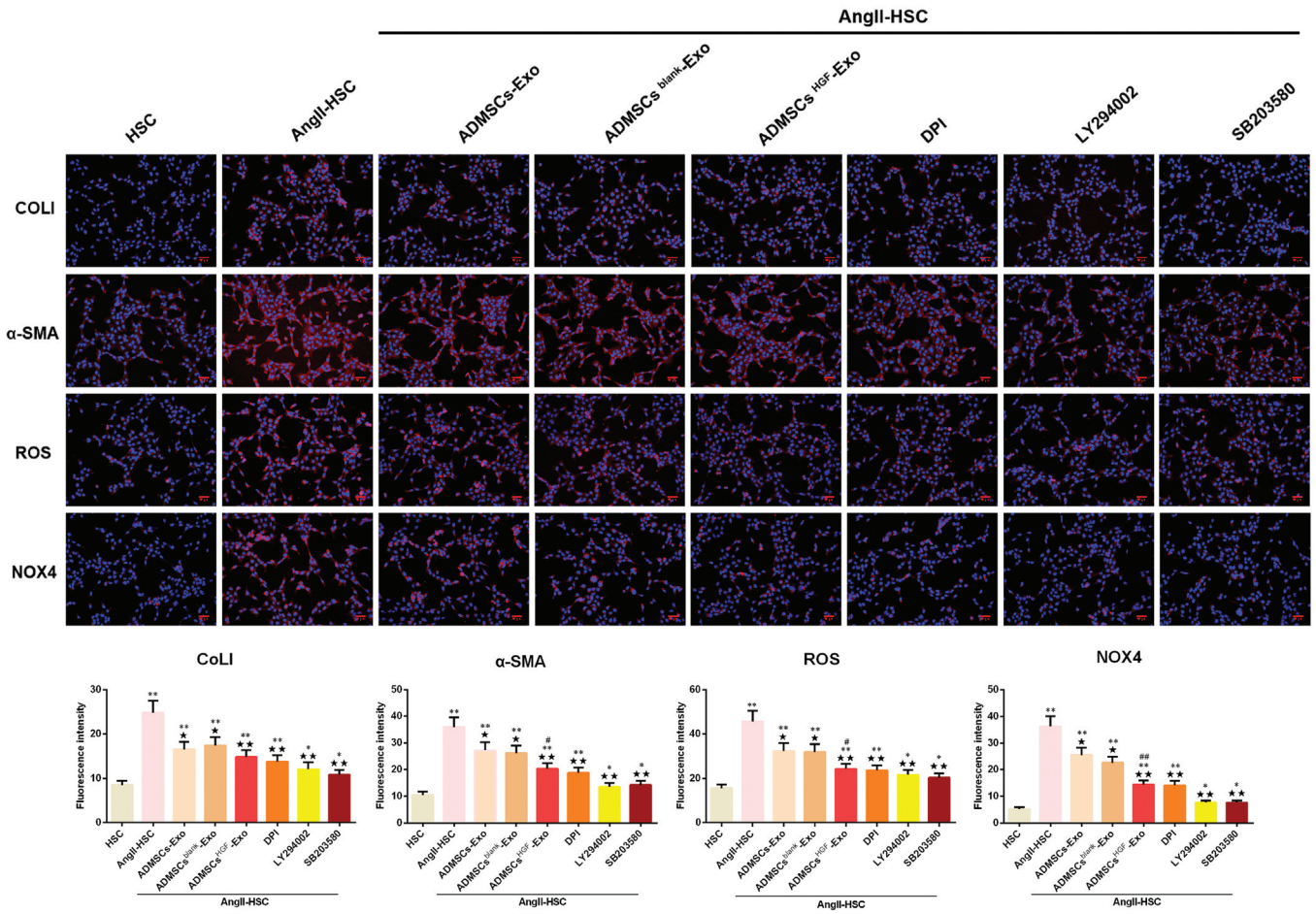

Fig. 4. ADMSCs^{HGF}-Exo decreased CoLI, α-SMA, ROS, and NOX4 expression in HSC-T6 cells. The detection of CoLI, α-SMA, ROS, and NOX4 expression in HSC-T6 cells was carried out by immunofluorescence assay. Data presented as mean ± SD, n=6. Compared with the HSC group, $^{*}p$<0.05, $^{**}p$<0.01; Compared with the AngII-HSC group, $^{★}p$<0.05, $^{★★}p$<0.01; Compared with the AngII-HSC + ADMSCsblank-Exo group, $^{\#}p$<0.05, $^{\#\#}p$<0.01. ADMSCs, Adipose-derived mesenchymal stem cells; HGF, hepatocyte growth factor; Exo, exosomes. CoLI: Collagen I; α-SMA: α-smooth muscle actin; ROS: Reactive oxygen species; NOX4: NADPH oxidase 4; NADPH: nicotinamide adenine dinucleotide phosphate.

decreased ALT, AST, and TBIL levels (p<0.01).

As shown in Fig. 7c, the liver lobules of the control group were clearly demarcated, and the hepatic sinusoids and confluent areas were normal. In the PBS group, hepatic lobules were poorly demarcated, with disorganized hepatocyte cords, extensive lamellar degeneration and eosinophilia, with necrosis and apoptotic vesicles of the hepatocytes, and hepatic sinusoids were narrowed or disappeared. The other three groups all improved liver tissue injury in mice, with a significantly lower liver tissue injury score (p<0.05 or p<0.01), the ADMSCs^{HGF}-Exo group being the most pronounced (p<0.01).

The results of Sirius red staining (Fig. 7d) showed that the control group had essentially no red collagen fibers except for the vessel wall, and the PBS group had obvious thick red fibers from the proliferation of collagen fibers outside the vessel wall. Collagen fiber accumulation in the liver tissue of mice in the PBS group was enhanced compared with the Control group (p<0.01). In contrast to the PBS group, there were red collagen fibers outside the vessel wall in the ADMSCs-

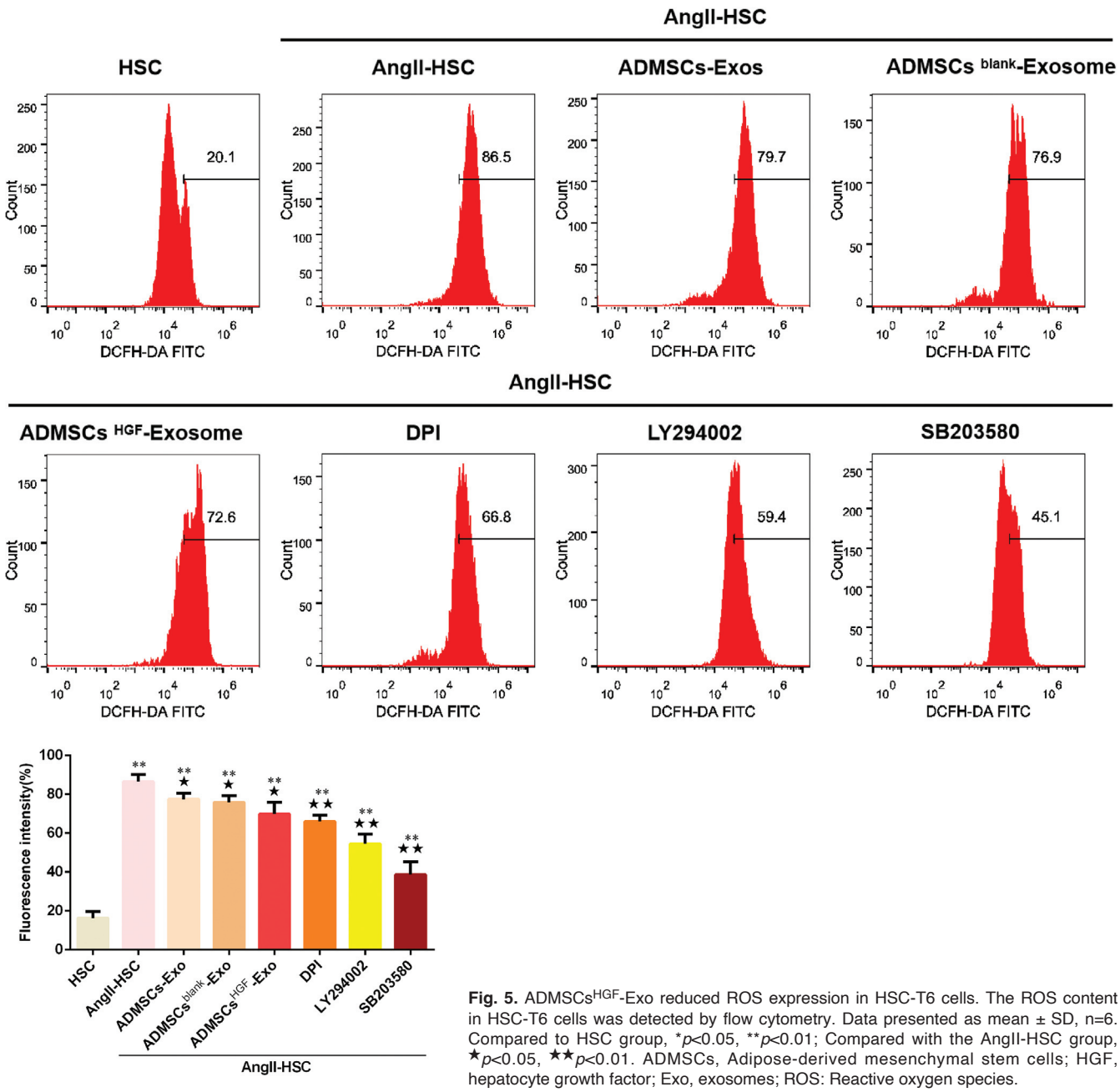

Fig. 5. ADMSCs^{HGF}-Exo reduced ROS expression in HSC-T6 cells. The ROS content in HSC-T6 cells was detected by flow cytometry. Data presented as mean ± SD, n=6. Compared to HSC group, *p<0.05, **p<0.01; Compared with the AngII-HSC group, ★p<0.05, ★★p<0.01. ADMSCs, Adipose-derived mesenchymal stem cells; HGF, hepatocyte growth factor; Exo, exosomes; ROS: Reactive oxygen species.

Exo and ADMSCs^{blank}-Exo groups, however, the fiber bundles were thinner and lighter in color than those in the PBS group. The ADMSCs^{HGF}-Exo group had only a small number of red collagen fibers outside the vessel wall with a slender nature. Collagen fiber accumulation was reduced in the ADMSCs-Exo, ADMSCs^{blank}-Exo, and ADMSCs^{HGF}-Exo groups compared with the PBS group (p<0.01).

The detection of lipid accumulation was made by Oil Red O staining (Fig. 7e). The relative area of lipid droplets in mouse liver tissues of the PBS group was greater than that of control mice (p<0.01), which was reduced after further ADMSCs-Exo, ADMSCs^{blank}-Exo, and ADMSCs^{HGF}-Exo intervention (p<0.05 or p<0.01).

ADMSCs^{HGF}-Exo diminished CoLI, α-SMA, and NOX4 expression in CCL4-treated mice liver tissues

CoLI, α-SMA, and NOX4 expression, detected by immunohistochemistry and western blot methods, were higher in liver tissues of mice in the PBS, ADMSCs-Exo, ADMSCs^{blank}-Exo, and ADMSCSs^{HGF}-Exo groups than in control mice (Fig. 8a-b, p<0.01). Relative to the PBS group, the expression of CoLI, α-SMA, and NOX4 in the ADMSCs-Exo, ADMSCs^{blank}-Exo, and ADMSCSs^{HGF}-Exo groups was decreased (p<0.05 or p<0.01). CoLI, α-SMA, and NOX4 expression were reduced in the ADMSCSs^{HGF}-Exo group compared with the ADMSCs^{blank}-Exo group (p<0.01).

ADMSCs^{HGF}-Exo downregulated oxidative stress and P-I3K, P-Akt, and P-P38MAPK protein expression in CCL4-treated mice

In Fig. 9a-h, serum levels of MDA were increased, and the levels of Na^+-K^+-ATPase, Ca^{2+}-Mg^{2+}-ATPase, SOD, GPx, CAT, GSH, and Mn-SOD were decreased in CCL4-treated mice of PBS, ADMSCs-Exo, ADMSCs^{blank}-Exo, and ADMSCs^{HGF}-Exo groups (p<0.05 or p<0.01). Serum levels of MDA in the ADMSCs-Exo, ADMSCs^{blank}-Exo, and ADMSCs^{HGF}-Exo groups were lower, whereas levels of Na^+-K^+-ATPase, Ca^{2+}-Mg^{2+}-ATPase, SOD, and CAT were higher than those of the PBS group (p<0.05 or p<0.01). Relative to the ADMSCs^{blank}-Exo group, ADMSCs^{HGF}-Exo exhibited decreased MDA levels but increased SOD, GSH, and Mn-SOD levels (p<0.05 or p<0.01).

As shown in Fig. 9i, the expression of P-I3K, P-Akt, and P-P38MAPK was higher in PBS, ADMSCs-Exo, ADMSCs^{blank}-Exo, and ADMSCs^{HGF}-Exo mice than in control mice (p<0.05 or p<0.01). Relative to the PBS group, P-I3K, P-Akt, and P-P38MAPK

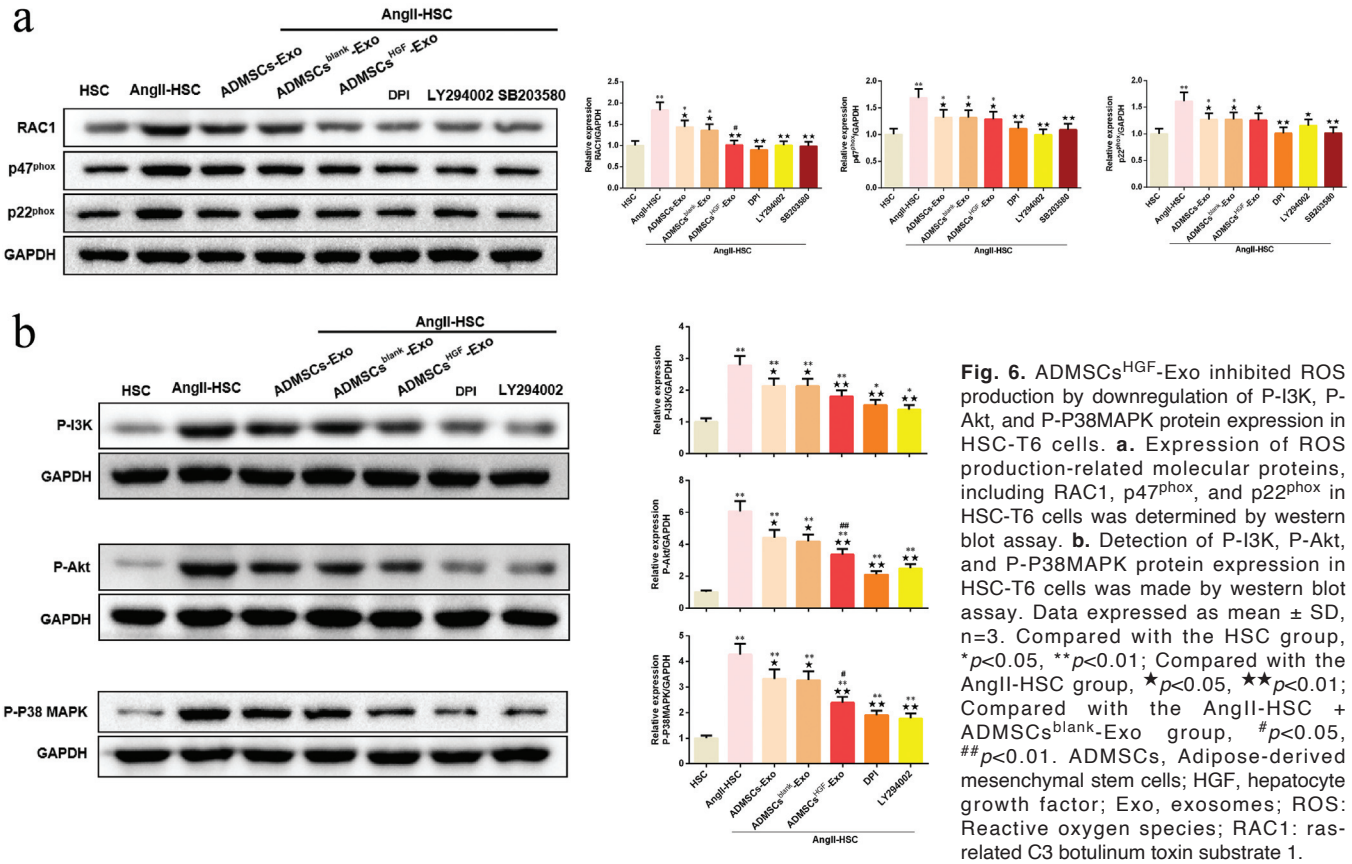

Fig. 6. ADMSCs^{HGF}-Exo inhibited ROS production by downregulation of P-I3K, P-Akt, and P-P38MAPK protein expression in HSC-T6 cells. **a.** Expression of ROS production-related molecular proteins, including RAC1, p47^{phox}, and p22^{phox} in HSC-T6 cells was determined by western blot assay. **b.** Detection of P-I3K, P-Akt, and P-P38MAPK protein expression in HSC-T6 cells was made by western blot assay. Data expressed as mean ± SD, n=3. Compared with the HSC group, *p<0.05, **p<0.01; Compared with the AngII-HSC group, ★p<0.05, ★★p<0.01; Compared with the AngII-HSC + ADMSCs^{blank}-Exo group, $^{\#}p$<0.05, $^{\#\#}p$<0.01. ADMSCs, Adipose-derived mesenchymal stem cells; HGF, hepatocyte growth factor; Exo, exosomes; ROS: Reactive oxygen species; RAC1: ras-related C3 botulinum toxin substrate 1.

expression in ADMSCs-Exo, ADMSCs^{blank}-Exo, and ADMSCs^{HGF}-Exo groups decreased (p<0.05 or p<0.01). Furthermore, there was lower P-I3K and P-Akt protein expression in the ADMSCs^{HGF}-Exo group than in the ADMSCs^{blank}-Exo group (p<0.05 or p<0.01).

Discussion

Liver fibrosis, triggered by various disease-causing factors, involves the overproduction of ECM, particularly collagen, in the liver (Kim et al., 2017). Slowing or reversing liver fibrosis can reduce the incidence of cirrhosis, its decompensated stage, and even hepatocellular carcinoma, enhancing patients' quality of life and extending survival (Yoon et al., 2016). Both *in vitro* and *in vivo* studies demonstrated that ADMSCs^{HGF}-Exo improved HSC cell viability, migratory capacity, and the expression of related proteins, such as ROS. Furthermore, it contributed to reducing hepatic oxidative stress levels, pathological damage, and collagen fibril accumulation.

Oxidative stress has been linked to HSC activation,

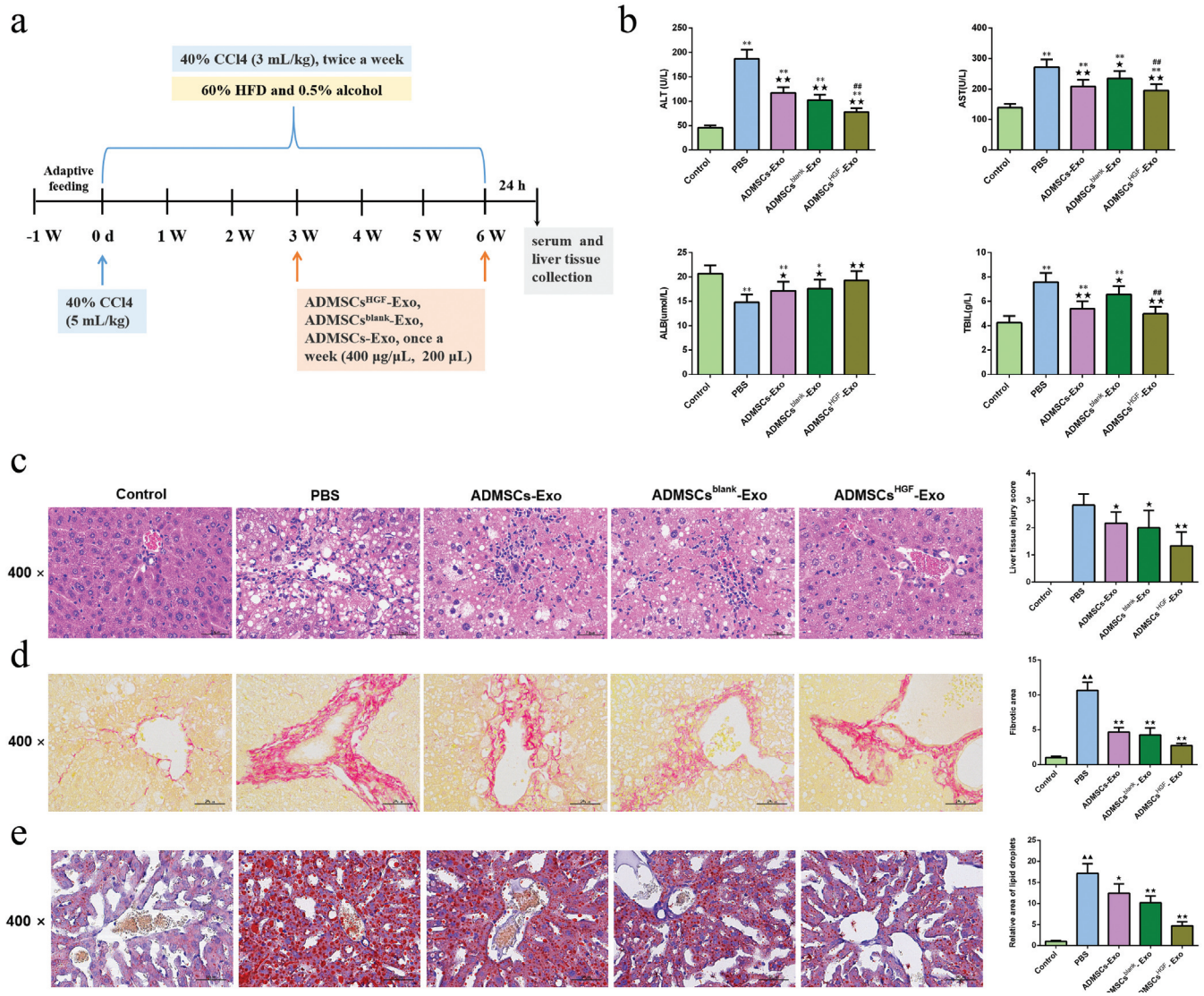

Fig. 7. ADMSCs^{HGF}-Exo ameliorated liver function biochemical indicators, liver tissue injury, fibrosis, and lipid accumulation in CCL4-treated mice. **a.** The flowchart of animal experiments. **b.** The measurement of serum ALT, AST, ALB, and TBIL levels in CCL4-treated mice was carried out by ELISA assay. **c.** The histopathological morphology of liver tissues in mice with acute liver injury was observed by HE staining. **d.** Observation of collagen fiber accumulation in liver tissues of mice with acute liver injury using Sirius red staining (400×). **e.** Oil Red O staining was employed to detect the lipid accumulation in liver tissues of mice (400×). Data expressed as mean ± SD, n=6. Compared with the HSC group, *p<0.05, **p<0.01; Compared with the AngII-HSC group, ★p<0.05, ★★p<0.01; Compared with the AngII-HSC + ADMSCs^{blank}-Exo group, $^{\#}p$<0.05, $^{\#\#}p$<0.01. ADMSCs, Adipose-derived mesenchymal stem cells; HGF, hepatocyte growth factor; Exo, exosomes; ALT: alanine aminotransferase; AST: aspartate transaminase; ALB: albumin; TBIL: total bilirubin. x 400.

with ROS playing a crucial role (Sánchez-Valle et al., 2012). NOX4-generated ROS can activate MAPK and PI3K/Akt signaling pathways, promoting HSC activation and inhibiting apoptosis, ultimately leading to liver fibrosis (Ikeda et al., 2011; Sancho et al., 2012). Increased NOX4 in liver fibrosis animal models has been associated with the promotion of liver fibrosis through the regulation of apoptosis and HSC activation (Luangmonkong et al., 2018). Moreover, increased HGF levels may inhibit inflammatory factors (Kanaya et al., 2021). Na^+-K^+-ATPase and Ca^{2+}-Mg^{2+}-ATPase are essential ATPases present in the mitochondrial membrane, serving as key indicators of cellular energy metabolism and functional impairment (Zhou et al., 2011). Hepatic fibrosis in rats led to higher MDA levels, with lower SOD, Na^+-K^+-ATPase, and Ca^{2+}-Mg^{2+}-ATPase levels (Wu et al., 2023). Early administration with cold water and ADMSCs-Exo protected the heart

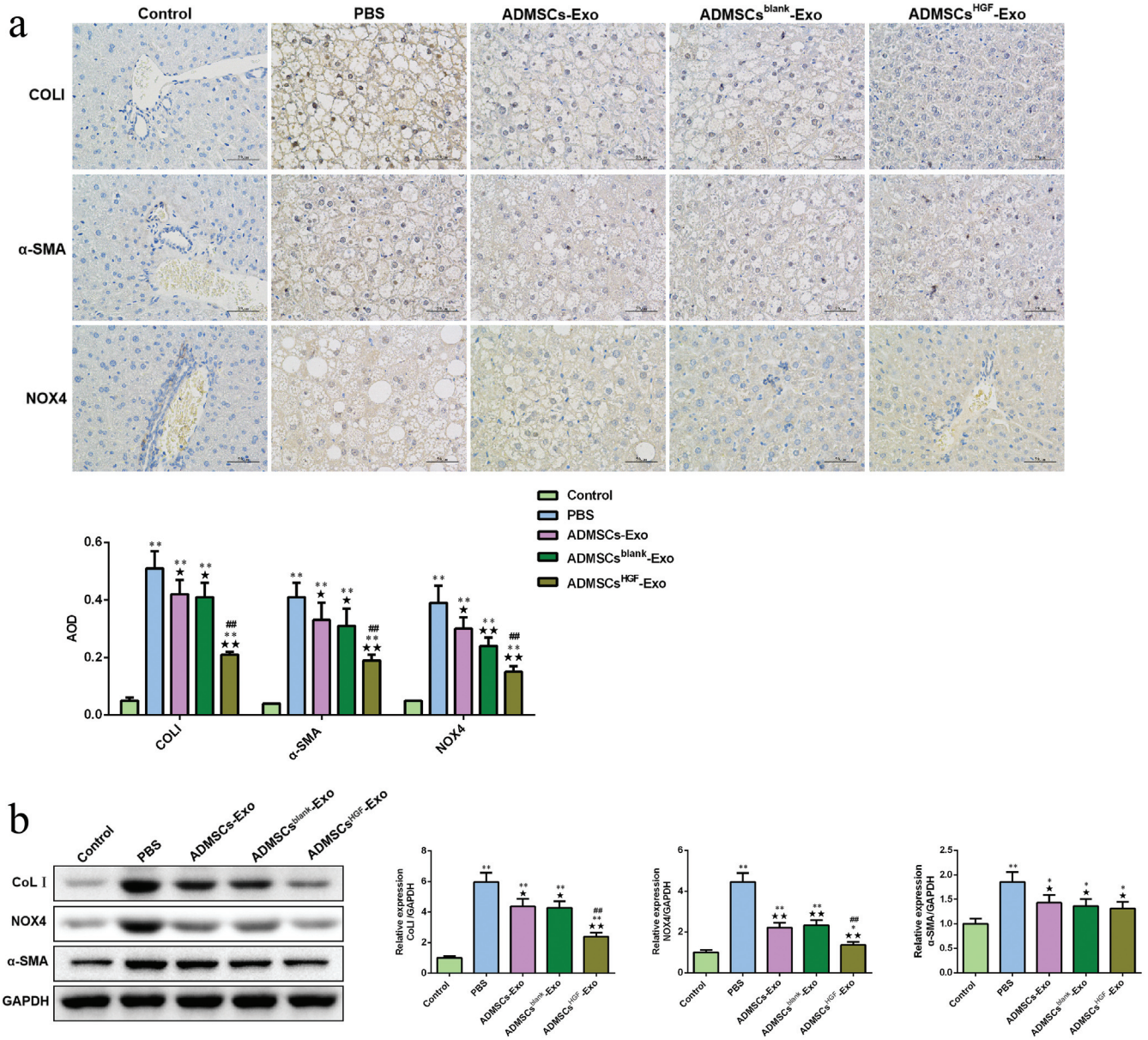

Fig. 8. ADMSCs^{HGF}-Exo diminished CoLI, α-SMA, and NOX4 expression in CCL4 mice liver tissues. Expression of CoLI, α-SMA, and NOX4 in mouse liver tissue was examined by immunohistochemistry **(a)** and western blot assay **(b)**. Data expressed as mean ± SD, n=6. Compared with the HSC group, $^*p<0.05$, $^{**}p<0.01$; Compared with the AngII-HSC group, $\bigstar p<0.05$, $\bigstar\bigstar p<0.01$; Compared with the AngII-HSC + ADMSCsblank-Exo group, $^{\#}p<0.05$, $^{\#\#}p<0.01$. ADMSCs, Adipose-derived mesenchymal stem cells; HGF, hepatocyte growth factor; Exo, exosomes; CoLI: Collagen I; α-SMA: α-smooth muscle actin; ROS: Reactive oxygen species; NOX4: NADPH oxidase 4; NADPH: nicotinamide adenine dinucleotide phosphate.

against ischemia-reperfusion injury by inhibition of ROS and NOX4 levels, as well as reduced left ventricular infarct/fibrotic/collagen-deposition areas (Chai et al., 2019). The above findings remain consistent with our results. Moreover, HGF overexpression promoted liver regeneration in CCL4-injured rats (Zhang et al., 2018). ADMSCs^{HGF}-Exo reduced the expression of ROS and PI3K/Akt/p38-MAPK-related pathway proteins in mouse liver tissues, and the inhibition of the p38/MAPK pathway was consistent with the known effects of HGF (Jones et al., 2005).

It has been indicated that DPI treatment reduces HSC viability (Liu et al., 2021), and SB203580 treatment decreases ROS levels, aiding in HSC recovery (Jung et al., 2016). Additionally, HGF has been reported to reduce NOX4 expression in perivascular cells (Cao et al., 2017). In our study, ADMSCs^{HGF}-Exo, DPI, LY294002, and SB203580 interventions all reversed AngII-induced effects. Interestingly, in this study, there were no significant differences in ROS content measured by flow cytometry, and p47^{phox} and p22^{phox} protein expression between ADMSCs^{HGF}-Exo and ADMSCs^{blank}-Exo cells, whereas lower ROS, p47^{phox} and p22^{phox} expression occurred in the ADMSCs-Exo group than in the AngII-HSC group. It was reasonable to infer that HGF might not be the unique regulator in ADMSCs-Exo. Wang et al. (2021) demonstrated that after ADMSCs-Exo intervention in oxygen-glucose deprivation-treated mouse cardiomyocytes, upregulated microRNA-671 directly targeted transforming growth factor beta receptor 2 (TGFBR2) and attenuated myocardial infarction by reducing Smad2 expression. In addition, ADMSCs-Exo-miRNA has been a hotspot in the field of skin wound repair and therapy, involved in the regulation of immune response, inflammatory response, reduction of fibrosis and collagen deposition (Ma et al., 2022). Subsequent studies could explore in depth the potential regulatory molecules in the

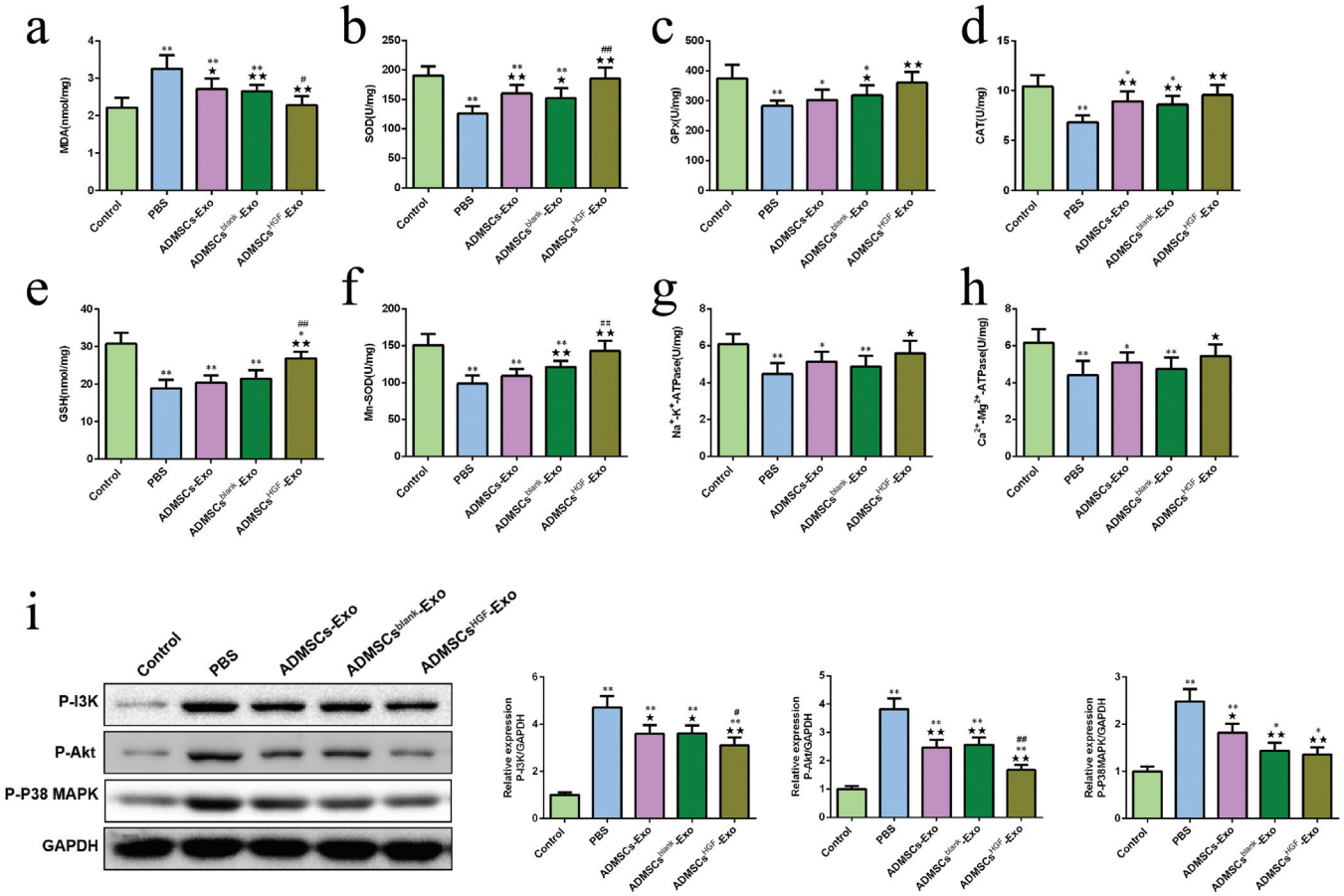

Fig. 9. ADMSCs^{HGF}-Exo downregulated oxidative stress and P-I3K, P-Akt, and P-P38MAPK protein expression in CCL4-treated mice. **a-h.** Detection of serum levels of MDA, SOD, GPx, CAT, GSH, Mn-SOD, Na^+-K^+-ATPase, and Ca^{2+}-Mg^{2+}-ATPase in mice. **i.** Measurement of P-I3K, P-Akt, and P-P38MAPK protein expression by western blot. Data expressed as mean ± SD, n=6. Compared with the HSC group, *p<0.05, **p<0.01; Compared with the AngII-HSC group, ★p<0.05, ★★p<0.01; Compared with the AngII-HSC + ADMSCs^{blank}-Exo group, $^{\#}p$<0.05, $^{\#\#}p$<0.01. ADMSCs, Adipose-derived mesenchymal stem cells; HGF, hepatocyte growth factor; Exo, exosomes; MDA: malondialdehyde; SOD: superoxide dismutase; GPx: glutathione peroxidase; CAT: catalase; GSH: glutathione; Mn-SOD: manganese superoxide dismutase.

amelioration of liver injury by ADMSCs-Exo.

Conclusion

This study demonstrates that ADMSCs^{HGF}-Exo play a regulatory role in oxidative stress during liver fibrosis through both *in vivo* and *in vitro* experiments, providing valuable insights for potential treatments of liver fibrosis.

Acknowledgments. None.

Funding. The authors declare that no funds, grants, or other support were received during the preparation of this manuscript.

Declaration of interests. The authors have no relevant financial or non-financial interests to disclose.

Author's contributions. Conception and design of the research: Hanyu Zhou; Acquisition of data: Yanyan Wu; Analysis and interpretation of data: Junchao Xue; Statistical analysis: Yanyan Wu and Junchao Xue; Drafting the manuscript: Hanyu Zhou; Revision of manuscript for important intellectual content: Liushenyan Yu; Approval of the final version of the manuscript to be published: All authors; Agreement to be accountable for all aspects of the work ensuring that questions related to the accuracy or integrity of the work are appropriately investigated and resolved: Hanyu Zhou, Yanyan Wu, Junchao Xue, Liushenyan Yu.

Ethics. All experimental procedures involved were performed according to protocols approved by the Institutional Animal Care and Use Committee at the Animal Experimentation Ethics Committee of Zhejiang Eyong Pharmaceutical Research and Development Center (SYXK-(Zhe)-2021-0033).

Data Availability Statement. The datasets generated and/or analyzed during the current study are available from the corresponding author upon reasonable request.

References

Asrani S.K., Devarbhavi H., Eaton J. and Kamath P.S. (2019). Burden of liver diseases in the world. J. Hepatol. 70, 151-171.

Atallah M.A.A., Elaidy S.M. and Tawfik M.K. (2018). Assessment of the possible roles of SB-269970 *versus* ketanserin on carbon tetrachloride-induced liver fibrosis in rats: Oxidative stress/TGF-β1-induced HSCs activation pathway. Pharmacol. Rep. 70, 509-518.

Cao Z., Ye T., Sun Y., Ji G., Shido K., Chen Y., Luo L., Na F., Li X., Huang Z., Ko J.L., Mittal V., Qiao L., Chen C., Martinez F.J., Fafil S. and Ding B.S. (2017). Targeting the vascular and perivascular niches as a regenerative therapy for lung and liver fibrosis. Sci. Transl. Med, 9, eaai8710.

Chai H.T., Sheu J.J., Chiang J.y., Shao P.L., Wu S.C., Chen Y.L., Li Y.C., Sung P.H., Lee F.Y. and Yip H.K. (2019). Early administration of cold water and adipose derived mesenchymal stem cell derived exosome effectively protects the heart from ischemia-reperfusion injury. Am. J. Transl. Res. 11, 5375-5389.

Chen X., Zhang D., Wang y., Chen K., Zhao L., Xu J., Jiang H. and Wang S. (2020). Synergistic antifibrotic effects of miR-451 with miR-185 partly by co-targeting EphB2 on hepatic stellate cells. Cell Death Dis. 11, 402.

Cordero-Espinoza L. and Huch M. (2018). The balancing act of the liver: tissue regeneration *versus* fibrosis. J. Clin. Invest. 128, 85-96.

Deng L., Kong X., Liu G., Li C., Chen H., Hong Z, Liu J. and Xia J. (2016). Transplantation of adipose-derived mesenchymal stem cells efficiently rescues thioacetamide-induced acute liver failure in mice. Transplant. Proc, 48, 2208-2215.

Dubey N.K., Mishra V.K. Dubey R., Deng Y.H., Tsai F.C. and Deng W.P. (2018). Revisiting the Advances in isolation, characterization and secretome of adipose-derived stromal/stem cells. Int. J. Mol. Sci. 19, 2200.

He L., Huang C., Wang H., Yang N., Zhang J., Xu L., Gu T., Li Z. and Chen Y. (2023). Galanin ameliorates liver inflammation and fibrosis in mice by activating AMPK/ACC signaling and modifying macrophage inflammatory phenotype. Front. Immunol. 14, 1161676.

Hu C., Wu Z. and Li L. (2020a). Pre-treatments enhance the therapeutic effects of mesenchymal stem cells in liver diseases. J. Cell. Mol. Med. 24, 40-49.

Hu X, Xu Q., Wan H., Hu Y., Xing S., Yang H., Gao Y. and He Z. (2020b). PI3K-Akt-mTOR/PFKFB3 pathway mediated lung fibroblast aerobic glycolysis and collagen synthesis in lipopolysaccharide-induced pulmonary fibrosis. Lab. Invest. 100, 801-811.

Ikeda R., Ishii K., Hoshikawa Y., Azumi J., Arakaki Y., Yasui T., Matsuura, S., Matsumi, Y., Kono R., Mizuta Y., Kirmasa A., Hisatome I., Friedman S.L., Kawasaki H. and Shiota G. (2011). Reactive oxygen species and NADPH oxidase 4 induced by transforming growth factor β1 are the therapeutic targets of polyenylphosphatidylcholine in the suppression of human hepatic stellate cell activation. Inflamm. Res. 60, 597-604.

Jones N.C., Tyner K.J., Nibarger L., Stanley H., Cornelison D.D., Fedorov Y.V. and Olwin B.B. (2005). The p38alpha/beta MAPK functions as a molecular switch to activate the quiescent satellite cell. J. Cell Biol, 169, 105-16.

Jung H., Kim D.O., Byun J.E. Kim W.S., Kim M.J., Song H.Y., Kim Y.K., Kang D.K., Park Y.J., Kim T.D., Yoon S.R., Lee H.G., Choi E.J., Min S.H. and Choi I. (2016). Thioredoxin-interacting protein regulates haematopoietic stem cell ageing and rejuvenation by inhibiting p38 kinase activity. Nat. Commun. 7, 13674.

Kanaya T., Miyagawa S., Kawamura T., Saki Y., Masada K., Nawa N., Ishida H., Narita J., Toda K., Kuratani T. and Sawa Y. (2021). Innovative therapeutic strategy using prostaglandin I2 agonist (ONO1301) combined with nano drug delivery system for pulmonary arterial hypertension. Sci. Rep. 11, 7292.

Kim J., Hyun J., Wang S., Lee C., Lee J.W., Moon E.Y., Cha H., Diehl A.M. and Jung Y. (2017). Thymosin beta-4 regulates activation of hepatic stellate cells via hedgehog signaling. Sci. Rep. 7, 3815.

Liu L., Zhang M., Hang L., Kong F., Yan H., Zhang Y., Feng X., Gao Y., Wang C., Ma H., Liu X., Zhan M., Pan Y., Xu H. and Niu J. (2020). Evaluation of a new point-of-care oral anti-HCV test for screening of hepatitis C virus infection. Virol. J. 17, 14.

Liu M., Wang D., Luo Y., Hu L., Bi Y., Ji J., Huang H., Wang G., Zhu L., Ma J., Kim E., Luo C.K., Abbruzzese J.L., Li X., Yang V.W., Li Z. and Lu W. (2021). Selective killing of cancer cells harboring mutant RAS by concomitant inhibition of NADPH oxidase and glutathione biosynthesis. Cell Death Dis. 12, 189.

Liu H., Wang X., Deng H., Huang H., Liu Y., Zhong Z. Shen L., Cao S., Ma X., Zhou Z., Chen D. and Peng G. (2023). Integrated transcriptome and metabolomics to reveal the mechanism of adipose mesenchymal stem cells in treating liver fibrosis. Int. J. Mol. Sci. 24, 16086.

Luangmonkong T., Suriguga T., Mutsaers H.A.M. Groothuis G.M.M., Olinga P. and Boersema M. (2018). Targeting oxidative stress for the treatment of liver fibrosis. Rev. Physiol. Biochem. Pharmacol.

175, 71-102.

Luo Y., He Y.Z., Wang Y.F., Xu Y.X. and Yang L. (2023). Adipose-derived mesenchymal stem cell exosomes ameliorate spinal cord injury in rats by activating the Nrf2/HO-1 pathway and regulating microglial polarization. Folia Neuropathol. 61, 326-335.

Ma J., Yong L., Lei P., Li H., Fang Y., Wang L., Chen H., Zhou Q., Wu W., Jin L., Sun D. and Zhang X. (2022). Advances in microRNA from adipose-derived mesenchymal stem cell-derived exosome: focusing on wound healing. J. Mater. Chem. B 10, 9565-9577.

Mo L., Hong S., Li Y., Hu Z. Han B. Wei Z. and Jia J. (2020). Sevoflurane inhibited inflammatory response induced by TNF-α in human trophoblastic cells through p38MAPK signaling pathway. J. Recept. Signal. Transduct. Res. 40, 218-223.

Mohamed R., Dayati P., Mehr R.N., Kamato D., Seif F., Babaahmadi-Rezael H. and Little P.J. (2019). Transforming growth factor-β1 mediated CHST11 and CHSY1 mRNA expression is ROS dependent in vascular smooth muscle cells. J. Cell. Commun. Signal. 13, 225-233.

Qiu B.F., Zhang G.Q., Xu F.M., Xu Q. and Xu T. (2019). Effect of the transdifferentiation of BECs into myofibroblasts on the pathogenesis of secondary cholestatic hepatic fibrosis. Exp. Ther. Med. 17, 2769-2776.

Ross J.J., Gherardi E., Mallorqui-Fernandez N., Bocci M., Sobkowicz A., Rees M., Rowe A. Ellmerich S., Massie I., Soeda J., Selden C. and Hodgson H. (2012). Protein engineered variants of hepatocyte growth factor/scatter factor promote proliferation of primary human hepatocytes and in rodent liver. Gastroenterology 142, 897-906.

Saidi R., Rajeshkumar R., Shariftbrizi A., Zimmerman A. and Walter O. (2015). Human adipose-derived mesenchymal stem cells promote liver regeneration. J. Invest. Surg. 28, 303-308.

Sánchez-Valle V., Chávez-Tapia N.C., Uribe M. and Méndez-Sánchez N. (2012). Role of oxidative stress and molecular changes in liver fibrosis: a review. Curr. Med. Chem. 19, 4850-4860.

Sancho P., Mainez J., Crosas-Molist E., Roncero C., Fernández-Rodríguez C.M. Pinedo F., Huber H., Eferl R., Mikulits W. and Fabregat I. (2012). NADPH oxidase NOX4 mediates stellate cell activation and hepatocyte cell death during liver fibrosis development. PLoS One 7, e45285.

Shiha G., Nabil A.G., Lotfy A., Soliman R., Hassan A.A., Ali I.S., Gad D.F. and Zahran F. (2020). Antifibrotic effect of combination of Nilotinib and stem cell-conditioned media on CCl4-Induced Liver Fibrosis. Stem Cells Int. 2020, 6574010.

Sorgun O. and Erbas O. (2023). Adipose-derived mesenchymal stem cells mitigate methotrexate-induced liver cirrhosis (fibrosis) model. Eur. Rev. Med. Pharmacol. Sci. 27, 11882-11889.

Wang X., Wang Y., Zhou X. and Liu F. (2019). Conditioned medium from adipose-derived stem cell inhibits Jurkat cell proliferation through TGF-β1 and p38/MAPK pathway. Anal. Cell. Pathol. 2019, 2107414.

Wang X., Zhu Y., Wu C., Liu W., He Y. and Yang Q. (2021). Adipose-derived mesenchymal stem cells-derived exosomes carry microRNA-671 to alleviate myocardial infarction through inactivating the TGFBR2/Smad2 axis. Inflammation 44, 1815-1830.

Watanabe Y., Tsuchiya A., Seino S., Kawata Y., Kojima Y., Ikarashi S., Starkey Lewis P.J., Lu W.Y., Kikuta J., Kawai H. Yamagiwa S., Forbes S.J. Ishii M. and Terai S. (2019). Mesenchymal Stem Cells and Induced Bone Marrow-Derived Macrophages Synergistically Improve Liver Fibrosis in Mice. Stem Cells Transl. Med, 8, 271-284.

Wu L., Liu J., Zheng C., Ma H., Cao X., Huang Z. and Tian K. (2023). The protective effect of SLNP on hepatic fibrosis induced by thioacetamide in rats. Curr. Pharm. Des. 29, 2988-2995.

Xiong J., Ding B., Zhu W., Xu L. and Yu S. (2023). Exosomes from adipose-derived mesenchymal stem cells protect against cyclophosphamide-induced cardiotoxicity in rats. Int. Heart J. 64, 935-944.

Yanan S., Bohan L., Shuaifeng S., Wendan T., Ma Z. and Wei L. (2023). Inhibition of Mogroside IIIE on isoproterenol-induced myocardial fibrosis through the TLR4/MyD88/NF-κB signaling pathway. Iran J. Basic Med. Sci. 26, 114-120.

Yao Y., Chen R., Wang G., Zhang Y. and Liu F. (2019). Exosomes derived from mesenchymal stem cells reverse EMT via TGF-β1/Smad pathway and promote repair of damaged endometrium. Stem Cell Res. Ther. 10, 225.

Yin C., Evason K.J., Asahina K and Stainer D.Y. (2013). Hepatic stellate cells in liver development, regeneration, and cancer. J. Clin. Invest. 123, 1902-1910.

Yoon Y.J. Friedman S.L. and Lee Y.A. (2016). Antifibrotic therapies: Where are we now? Semin. Liver Dis. 36, 87-98.

Zedan Z.K. and Al-Ameri S.H.A. (2023). *In vitro* study of primary isolation and culture of adipose-derived stem cells and induction of chondrogenic differentiation. Arch. Razi Inst. 78, 125-133.

Zhang L., Li R., Rong W., Han M., Cui C., Feng Z., Sun X. and Jin S. (2018). Therapeutic effect of hepatocyte growth factor-overexpressing bone marrow-derived mesenchymal stem cells on CCl4-induced hepatocirrhosis. Cell Death Dis. 9, 1186.

Zhou L., Aon M.A. Liu T. and O'Rourke B. (2011). Dynamic modulation of Ca^{2+} sparks by mitochondrial oscillations in isolated guinea pig cardiomyocytes under oxidative stress. J. Mol. Cell Cardiol. 51, 632-639.

Accepted September 18, 2024